Kondo physics of the Anderson impurity model by distributional exact diagonalization

S. Motahari, R. Requist, and D. Jacob*

Max-Planck-Institut für Mikrostrukturphysik, Weinberg 2, 06120 Halle, Germany

(Received 12 August 2016; revised manuscript received 1 November 2016; published 14 December 2016)

The distributional exact diagonalization (DED) scheme is applied to the description of Kondo physics in the Anderson impurity model. DED maps Anderson's problem of an interacting impurity level coupled to an infinite bath onto an ensemble of finite Anderson models, each of which can be solved by exact diagonalization. An approximation to the self-energy of the original infinite model is then obtained from the ensemble-averaged self-energy. Using Friedel's sum rule, we show that the particle number constraint, a central ingredient of the DED scheme, ultimately imposes Fermi liquid behavior on the ensemble-averaged self-energy, and thus is essential for the description of Kondo physics within DED. Using the numerical renormalization group (NRG) method as a benchmark, we show that DED yields excellent spectra, both inside and outside the Kondo regime for a moderate number of bath sites. Only for very strong correlations ($U/\Gamma \gg 10$) does the number of bath sites needed to achieve good quantitative agreement become too large to be computationally feasible.

DOI: 10.1103/PhysRevB.94.235133

I. INTRODUCTION

The Anderson impurity model (AIM) [1] plays a central role in the understanding of one of the most intriguing many-body phenomena, the Kondo effect [2], and is also at the heart of dynamical mean-field theory (DMFT) [3–6]. The numerical renormalization group (NRG) method [7] solves the model exactly, but is computationally very demanding and unable to make use of the strongest form of parallelization. Another numerically exact method for solving the AIM is the continuous-time quantum Monte Carlo (CTQMC) algorithm [8], which can be parallelized efficiently, but has the disadvantage of working in imaginary time. The necessary analytical continuation back to the real axis brings about artifacts in the spectral function. Another serious drawback of CTQMC is its restriction to relatively high temperatures, making this approach of limited use for the study of low-temperature phenomena such as the Kondo effect.

A number of approximate methods for solving the Anderson model exist as well. The noncrossing approximation (NCA) [9,10] and one-crossing approximation (OCA) [11,12], for example, consist of a diagrammatic expansion around the atomic limit, summing only a subset of diagrams to infinite order. Both NCA and OCA yield qualitatively correct spectra for not too low temperatures. While the simpler NCA strongly underestimates the width of the Kondo peak, the vertex corrections within OCA lead to a quantitatively correct estimate of the Kondo scale. At lower temperatures, both NCA and OCA show spurious non-Fermi-liquid behavior, leading to artifacts in the spectra [13,14]. Many other approximate schemes for solving the AIM exist [15–19], though all are burdened with some kind of limitation.

Common to most approximation schemes is the solution of the infinite AIM, consisting of an impurity level coupled to an infinite and continuous bath representing a conduction electron band. A different route is to replace the infinite AIM by a finite one that can then be solved by numerical diagonalization [20,21]. The infinite and continuous conduction electron bath is approximated by a finite number of discrete bath levels. When this approach is adopted in DMFT as an impurity solver, it yields thermodynamic and static quantities in very good agreement with, e.g., numerically exact CTQMC, but often leads to artifacts in the spectral functions stemming from finite-size effects. Especially in the Kondo regime, the discrete nature of the conduction electron bath in the exact-diagonalization approach seriously compromises the correctness of the impurity density of states, a key observable [22] in the scanning tunneling spectroscopy of surface Kondo systems such as Ce on silver [23] or Co on gold [24] and copper [25–33] surfaces.

Recently, Granath and Strand have proposed a method for solving the AIM that overcomes the problem of discretization artifacts. The distributional exact diagonalization (DED) approach [34,35] maps the infinite Anderson model onto an *ensemble* of finite Anderson models instead of a single effective finite Anderson model. The ensemble average of the self-energies of the finite Anderson models provides a smooth approximation to the self-energy of the original infinite Anderson model that is also free of finite-size artifacts. An advantage of the DED method in comparison with NRG is its straightforward and efficient large-scale parallelization. Different strategies for improving direct diagonalization methods have been proposed recently. In one, a careful selection of basis states makes it possible to include a large number of bath levels [36]. In another, the parameters of an effective finite Anderson model are variationally optimized [37].

Here we show that the DED approach gives an excellent description of the Anderson model inside and outside the Kondo regime, except for very strong correlations. We find that already for a very small number of 1–2 bath sites, the spectra are in good qualitative agreement with exact spectra calculated by NRG. For a moderate number of 5–7 bath sites the agreement becomes excellent, also with regard to the width of the Kondo peak. Only for very strong correlation strength ($U/\Gamma \gg 10$) does the number of bath sites necessary to obtain quantitative results become computationally prohibitive due to the exponential growth of the Kondo screening cloud with correlation strength.

*djacob@mpi-halle.mpg.de

The paper is organized as follows. In Sec. II we first review the DED method, originally introduced by Granath and Strand, and then elucidate the role of the particle number constraint that is needed to make the method work. In Sec. III we apply the DED method to the single-orbital AIM, both in the particle-hole (ph) symmetric case (Sec. III A) and in the presence of asymmetry (Sec. III B). Finally, in Sec. IV we conclude the paper with a discussion of the results and a perspective on using DED for more general types of Anderson impurity models.

II. METHOD

A. Review of the DED algorithm

We consider the AIM of a single interacting impurity level coupled to an infinite bath of conduction electrons:

$$H = \epsilon_d n_d + U n_{d\uparrow} n_{d\downarrow} + \sum_{\sigma,k} \epsilon_k \, c^\dagger_{k\sigma} c_{k\sigma} + \sum_{\sigma,k} V_k \, (d^\dagger_\sigma c_{k\sigma} + c^\dagger_{k\sigma} d_\sigma) \tag{1}$$

with d_σ ($d^\dagger_\sigma$) the annihilation (creation) operator for the impurity level d and spin σ, $c_{k\sigma}$ ($c^\dagger_{k\sigma}$), the annihilation (creation) operators for bath levels k and spin σ, $n_{d\sigma} = d^\dagger_\sigma d_\sigma$, $n_d = \sum_\sigma n_{d\sigma}$, ϵ_d the bare impurity level energy, U the on-site Coulomb repulsion at the impurity, ϵ_k the band energy of conduction electrons, and V_k the coupling between the impurity level d and conduction electron k. The chemical potential μ is assumed to be zero throughout the paper.

The general idea of the DED approach is to map the infinite Anderson model to an ensemble of relatively small *finite* Anderson models that can be diagonalized exactly. Our starting point is the noninteracting retarded Green's function:

$$G_0(\omega) = \frac{1}{\omega^+ - \epsilon_d - \Sigma_0 - \Delta(\omega)}, \tag{2}$$

where $\Delta(\omega)$ is the hybridization function $\Delta(\omega) = \sum_k \frac{(V_k)^2}{\omega^+ - \epsilon_k}$, describing the renormalization (real part) and broadening (imaginary part) of the impurity level due to the coupling to the conduction electron bath. For all calculations presented here we assume a flat hybridization function, i.e., $\Delta(\omega) = -i\Gamma$ (wide-band limit), but the approach is not limited in that respect.

The parameter Σ_0 can be understood as an effective one-body potential for the noninteracting reference system. Its exact role will be elucidated later in the context of the constraint (see Sec. II B). Anticipating our later discussion, we mention here that Fermi liquid theory considerations suggest that Σ_0 should be the real part of the interacting self-energy at the Fermi level. In including Σ_0 already at this stage, and interpreting it as an effective one-body potential, our approach deviates somewhat from the one originally proposed by Granath and Strand [34] (see Sec. II B for a detailed discussion).

Next, G_0 is represented by a large number M of poles b_i on the real axis, thereby effectively discretizing the conduction electron bath:

$$G_0(\omega) = \sum_{i=1}^{M} \frac{a_i}{\omega^+ - b_i}. \tag{3}$$

Here a_i are the residues corresponding to the poles b_i which have to be normalized according to $\sum a_i = 1$. We then divide the poles into N groups of size n ($Nn = M$):

$$G_0(\omega) = \frac{1}{N} \sum_{\nu=1}^{N} \sum_{i=1}^{n} \frac{a_i^\nu}{\omega^+ - b_i^\nu} = \frac{1}{N} \sum_\nu G_0^\nu(\omega), \tag{4}$$

where n is a relatively small integer number that ultimately determines the size of the finite AIM, and N the number of finite-size Anderson model samples in the ensemble. Now the residues in *each group* have to be normalized according to $\sum_{i=1}^n a_i^\nu = 1$ for all $\nu = 1 \ldots N$.

The poles representing $G_0(\omega)$ are generated randomly using the noninteracting spectral density $\rho_0(\omega) = -\mathrm{Im}[G_0(\omega)]/\pi$ as the probability distribution. Each set ν of n such randomly chosen poles then uniquely defines the noninteracting part of a finite-size (n sites) Anderson model:

$$H_0^\nu = \epsilon_0^\nu \sum_\sigma d^\dagger_\sigma d_\sigma + \sum_{\sigma,k=1}^{n-1} V_k^\nu (d^\dagger_\sigma c_{k\sigma} + c^\dagger_{k\sigma} d_\sigma) + \sum_{\sigma,k=1}^{n-1} \epsilon_k^\nu \, c^\dagger_{k\sigma} c_{k\sigma}. \tag{5}$$

The mapping from the set of poles to the parameters of the finite Anderson model is achieved by equating $G_0^\nu(\omega)$ and the impurity Green's function (GF) corresponding to H_0^ν:

$$\sum_{i=1}^{n} \frac{a_i^\nu}{\omega^+ - b_i^\nu} = \left(\omega^+ - \epsilon_0^\nu - \sum_{k=1}^{n-1} \frac{\left(V_k^\nu\right)^2}{\omega^+ - \epsilon_k^\nu} \right)^{-1}, \tag{6}$$

where the residues are taken to be constant with $a_i^\nu = 1/n$. Note that since the poles b_i^ν are chosen to be distributed randomly according to the probabilities $\rho_0(b_i^\nu)$, the seemingly reasonable choice $a_i^\nu \sim \rho_0(b_i^\nu)$ for the residues is actually wrong as it would lead to a sampled noninteracting DOS different from $\rho_0(\omega)$. The bath energy levels ϵ_k^ν can now be found from the roots of G_0^ν,

$$G_0^\nu\left(\omega = \epsilon_k^\nu\right) = 0 \quad \forall\, k = 1, \ldots, n-1, \tag{7}$$

while the hoppings V_k^ν between the impurity and the bath levels are obtained from the derivative of G_0^ν at the bath level energies as

$$\left.\frac{dG_0^\nu}{d\omega}\right|_{\epsilon_k^\nu} = -\frac{1}{\left(V_k^\nu\right)^2} \quad \forall\, k = 1, \ldots, n-1. \tag{8}$$

Finally, the impurity level energy is obtained from the mean value of sampled poles:

$$\epsilon_0^\nu = \sum_{i=1}^{n} a_i^\nu b_i^\nu = \frac{1}{n} \sum_{i=1}^{n} b_i^\nu. \tag{9}$$

In the next step, the interacting finite Anderson model is obtained by adding the interaction part, and, importantly,

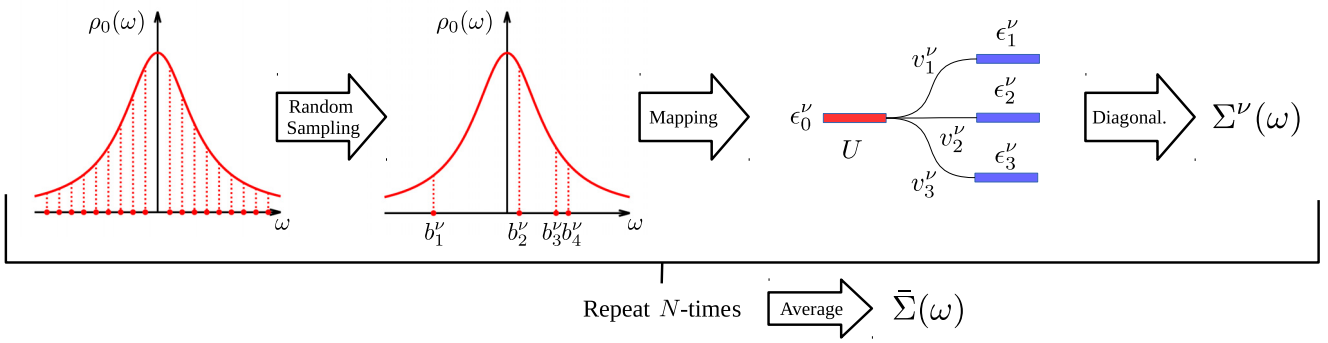

FIG. 1. Schematic representation of the DED method. The noninteracting density of the impurity level $\rho_0(\omega)$ is interpreted as a probability distribution for the poles of the noninteracting Green's function $G_0(\omega)$. A finite number of poles b_i^ν is then generated randomly according to the distribution $\rho_0(\omega)$. The selected n poles uniquely define a finite Anderson model H^ν with $n-1$ bath sites. Diagonalization of H^ν yields the self-energy $\Sigma^\nu(\omega)$ corresponding to the finite Anderson model. This process is repeated many times (N). An approximation to the self-energy of the original infinite Anderson model (1) is obtained from the ensemble average of the self-energies of the finite Anderson model samples (13).

subtracting out the effective one-body potential Σ_0, to avoid double counting of interactions:

$$H^\nu = H_0^\nu + U n_{d\uparrow} n_{d\downarrow} - \Sigma_0 n_d. \tag{10}$$

Hence we see that Σ_0 does not really play a role yet. The role of Σ_0 will become clear later in the context of the constraint (see Sec. II B). For later convenience we also define the bare impurity level $\epsilon_d^\nu = \epsilon_0^\nu - \Sigma_0$ of the finite model. Note that $\epsilon_d^\nu \to \epsilon_d$ in the limit of $n \to \infty$.

The finite Anderson model Hamiltonian H^ν is now diagonalized numerically. This yields the many-body eigenstates $|m^\nu\rangle$ and corresponding eigenenergies E_m^ν. The GF for the impurity level is then obtained from the Lehmann representation:

$$G_\sigma^\nu(\omega) = \sum_m \frac{|\langle m^\nu|d_\sigma|0^\nu\rangle|^2}{\omega^+ + E_m^\nu - E_0^\nu} + \sum_m \frac{|\langle m^\nu|d_\sigma^\dagger|0^\nu\rangle|^2}{\omega^+ + E_0^\nu - E_m^\nu}, \tag{11}$$

where $|0^\nu\rangle$ and E_0^ν denote the ground state and corresponding ground state energy [38]. In the case of a degenerate ground state the GF would be obtained from the corresponding ensemble average over the ground state manifold. Note, however, that the particle constraint discussed in Sec. II B ensures that the ground state is actually a singlet state. The corresponding self-energy of the finite Anderson model is

$$\Sigma_\sigma^\nu(\omega) = \left[G_0^\nu(\omega)\right]^{-1} - \left[G_\sigma^\nu(\omega)\right]^{-1} + \Sigma_0. \tag{12}$$

This process of generating finite Anderson model Hamiltonians H^ν and calculating their self-energies Σ_σ^ν is repeated N times. Finally, an approximation to the self-energy of the original *infinite* Anderson model is obtained from the ensemble average

$$\bar{\Sigma}_\sigma(\omega) = \frac{1}{N}\sum_{\nu=1}^{N} \Sigma_\sigma^\nu(\omega). \tag{13}$$

An approximation to the corresponding interacting GF is obtained from $G_\sigma(\omega) = [\omega^+ - \epsilon_d - \bar{\Sigma}_\sigma(\omega) - \Delta(\omega)]^{-1}$. As observed by Granath and Strand, obtaining an approximation to the GF of the infinite Anderson model by directly averaging the $G_\sigma^\nu(\omega)$ is not an option, since the sample-averaged interacting and noninteracting GFs $\bar{G}_\sigma(\omega) = \frac{1}{N}\sum_\nu G_\sigma^\nu(\omega)$ and $\bar{G}_0(\omega) = \frac{1}{N}\sum_\nu \bar{G}_\sigma^\nu(\omega)$, respectively, do not form a proper pair of interacting and noninteracting GFs connected by the Dyson equation [34]. Figure 1 shows a schematic representation summarizing the main steps of the DED procedure.

B. Role of the constraint

Granath and Strand found that in order to obtain valid spectra not all randomly generated Anderson models can be accepted. As can be seen in Fig. 2(a) (red dashed line), the Kondo peak is practically nonexistent and the Hubbard side peaks are overestimated when all randomly generated finite Anderson model samples contribute equally. In order to deal with this problem, Granath and Strand introduced a constraint comparing the number of particles in the interacting and noninteracting systems. More precisely, a sample ν is only accepted if

$$N^\nu \overset{(!)}{=} N_0^\nu, \tag{14}$$

where N^ν is the number of particles of the ground state of the interacting model H^ν and N_0^ν that of the noninteracting

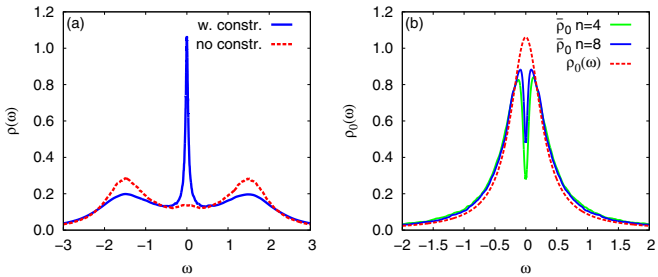

FIG. 2. Effect of constraint: (a) Comparison of spectra calculated with (blue line) and without (red dashed line) imposing the particle number constraint for $n = 4$ sites, $\Gamma = 0.3$, $U = 3$, $\epsilon_d = -U/2$. (b) Comparison of sampled noninteracting DOS $\bar{\rho}_0(\omega) = -\mathrm{Im}\bar{G}_0(\omega)/\pi$ for different number of sites with original Lorentzian noninteracting DOS $\rho_0(\omega)$.

model H_0^ν. As can be seen in Fig. 2(a) (blue line), applying the constraint indeed recovers the full height of the Kondo peak at the Fermi level and lowers the Hubbard side peaks. The effect of the constraint on the sampled noninteracting DOS is to deplete the DOS around the Fermi level as can be seen in Fig. 2(b). As the number of sites n increases the effect of the constraint becomes smaller.

In order to elucidate the role played by the constraint, we now consider Friedel's sum rule for the Anderson model [2,39,40] which relates the impurity charge $n_{\mathrm{imp},\sigma}$ to the scattering phase shift at the Fermi level. For a finite Anderson model sample ν we can write

$$n^\nu_{\mathrm{imp},\sigma} = \eta^\nu_\sigma(\epsilon_\mathrm{F})/\pi, \tag{15}$$

where the scattering phase shift η^ν_σ is given by

$$\eta^\nu_\sigma(\omega) = \frac{\pi}{2} - \tan^{-1}\left(\frac{\omega - \epsilon^\nu_d - \mathrm{Re}\,\Sigma^\nu_\sigma(\omega) - \mathrm{Re}\,\Delta^\nu(\omega)}{\mathrm{Im}\,\Sigma^\nu_\sigma(\omega) + \mathrm{Im}\,\Delta^\nu(\omega)}\right). \tag{16}$$

As we are considering a *finite* Anderson model, the hybridization function

$$\Delta^\nu(\omega) = \sum_k \frac{\left|V^\nu_k\right|^2}{\omega^+ - \epsilon^\nu_k}, \tag{17}$$

which describes the coupling of the impurity level with the bath levels, is the sum of a finite number of poles, and thus nonconstant by construction. In this case the impurity charge $n^\nu_{\mathrm{imp},\sigma}$ comprises not only the impurity level occupancy $n^\nu_{d,\sigma}$ but also the additional scattering-induced charge $\delta n_{\mathrm{imp},\sigma}$:

$$\begin{aligned} n^\nu_{\mathrm{imp},\sigma} &= n^\nu_{d,\sigma} + \delta n^\nu_{\mathrm{imp},\sigma} \\ &= -\int_{-\infty}^{\epsilon_\mathrm{F}} \frac{d\omega}{\pi}\,\mathrm{Im}\left(G^\nu_\sigma(\omega) + \sum_k \left[g^\nu_k(\omega)\right]^2 T^\nu_{k\sigma}(\omega)\right), \end{aligned} \tag{18}$$

where $g^\nu_k(\omega) = 1/(\omega^+ - \epsilon^\nu_k)$ is the propagator for the *isolated* (i.e., not connected to the impurity) bath level k, and $T^\nu_{k\sigma}(\omega) = V^\nu_k G^\nu_\sigma(\omega) V^\nu_k$ is the scattering T matrix.

The total number of electrons N^ν for sample ν is given by the sum of the impurity charge $n^\nu_{\mathrm{imp},\sigma}$ and the occupation of the the *isolated* bath levels $n^\nu_{\mathrm{bath}} = -\mathrm{Im}\int_{-\infty}^{\epsilon_\mathrm{F}} d\omega \sum_k g_k(\omega)/\pi$. Since the occupation of the *isolated* bath levels is the same in the interacting and noninteracting system, the particle constraint ultimately imposes that the impurity charge and in turn the phase shifts are the same for the interacting and noninteracting models:

$$n^\nu_{\mathrm{imp},\sigma} = \frac{\eta^\nu_\sigma(\epsilon_\mathrm{F})}{\pi} \overset{\text{constr.}}{=} n^\nu_{\mathrm{imp},\sigma,0} = \frac{\eta^\nu_{\sigma,0}(\epsilon_\mathrm{F})}{\pi}, \tag{19}$$

where the phase shift of the noninteracting system is given by

$$\eta^\nu_{0,\sigma}(\omega) = \frac{\pi}{2} - \tan^{-1}\left(\frac{\omega - \epsilon^\nu_0 - \mathrm{Re}\Delta^\nu(\omega)}{\mathrm{Im}\Delta^\nu(\omega)}\right). \tag{20}$$

It is here that the effective potential Σ_0 included in the noninteracting GF (2) enters in the constraint: Since $\epsilon^\nu_0 = \epsilon^\nu_d + \Sigma_0$ it determines the phase shift $\eta^\nu_{0,\sigma}(\epsilon_\mathrm{F})$ and consequently the impurity charge $n^\nu_{\mathrm{imp},\sigma,0}$ of the noninteracting reference system.

Hence the constraint guarantees that only self-energies $\Sigma^\nu_\sigma(\omega)$ which have the same phase shift as the corresponding noninteracting model contribute to the ensemble average (13). A closer look at the phase shifts η^ν_σ and $\eta^\nu_{0,\sigma}$ of individual finite Anderson model samples ν further reveals that the constraint really establishes a 1:1 correspondence between the excitations of the interacting Hamiltonian H^ν and the corresponding noninteracting one H^ν_0, as required by Fermi liquid theory (see Appendix A for details). When the constraint is not fulfilled, the 1:1 correspondence with the noninteracting system cannot be established, because the ground state of the interacting system has an odd number of electrons ($N^\nu = N^\nu_0 \pm 1$) and thus is a doublet state ($S = 1/2$), while the noninteracting system must have an even number of electrons (single-particle levels are either doubly occupied or unoccupied), and thus has a singlet ground state ($S = 0$). Thus the constraint ultimately enforces that individual Anderson model samples contributing to the self-energy average (13) comply with Nozieres' Fermi liquid picture [41] of the Kondo effect in the strong-coupling regime: the impurity spin locks into a total spin singlet state with a few conduction electron bath levels, and the remaining conduction electrons interact weakly with the singlet state, thus leading to Fermi liquid behavior. Since Friedel's sum rule is directly related to the height of the Kondo peak at the Fermi energy, the particle constraint ultimately leads to the recovery of the unitary limit for the interacting spectral function, and consequently to the recovery of Fermi liquid behavior.

The interpretation of the constraint as a sample-wise enforcement of Fermi liquid behavior suggests that the parameter Σ_0 should be interpreted as an effective one-body potential that can be identified with the real part of the (yet to be determined) many-body self-energy:

$$\Sigma_0 \equiv \mathrm{Re}\bar{\Sigma}(\epsilon_\mathrm{F}). \tag{21}$$

This conjecture can be further justified by considering the exact limit of the DED approach: taking the number of poles $n \to \infty$, the original infinite Anderson model is recovered. Since now there is only one sample, the constraint must be fulfilled for this one sample, hence the phase shift of the interacting and corresponding noninteracting model must match exactly, leading to

$$\tan^{-1}\left(\frac{\epsilon_d + \mathrm{Re}\Sigma(\epsilon_\mathrm{F}) - \epsilon_\mathrm{F}}{\Gamma}\right) \overset{(!)}{=} \tan^{-1}\left(\frac{\epsilon_d + \Sigma_0 - \epsilon_\mathrm{F}}{\Gamma}\right),$$

which implies (21).

Since the self-energy itself is not known prior to the calculation, Σ_0 has to be determined self-consistently, starting with some initial guess for Σ_0, for example the Hartree shift $\Sigma_0 \equiv U n_d/2$ with n_d being the Hartree-Fock occupancy. This is where our approach slightly differs from the one originally proposed by Granath and Strand, which takes Σ_0 as an adjustable parameter to be fixed by demanding that the interacting and noninteracting impurity occupancy n_d be the same.

III. RESULTS

In the following we present results for the AIM described by Eq. (1), assuming a constant hybridization function $\Delta(\omega) =$

$-i\Gamma$. The noninteracting density of states $\rho_0(\omega)$ is thus a Lorentzian centered at $\epsilon_d + \Sigma_0$ of width 2Γ. To resolve the interacting spectral functions we use a logarithmic mesh, and a frequency-dependent Lorentzian broadening scheme where an imaginary part proportional to the frequency is added to the frequency argument in the denominators of the Green's functions, i.e., $\omega^+ = \omega + i\eta_1|\omega|$ with $\eta_1 = 0.02$. The NRG calculations were performed with the NRG Ljubljana code [42], using the z-averaging technique [43] with $z = 64$. For all calculations, we set the conduction-band half-width to $D = 10$, the logarithmic discretization parameter to $\Lambda = 2$, and determined the number of states kept at each iteration by an energy cutoff of $10\omega_N$ (ω_N is the characteristic energy scale of iteration N); the maximum number of states kept was 6600 counting multiplicities. Log-Gaussian broadening [44] was used in the calculation of the spectral functions with a width parameter of $\alpha = 0.2$ for the asymmetric AIM. For the symmetric AIM, α was varied between 0.15 for small Γ and 0.35 for large Γ.

A. Symmetric Anderson model

First, we study the AIM at particle-hole symmetry, $\epsilon_d = -U/2$ and $\langle n_d\rangle = 1$. In this case the real part of the self-energy at the Fermi level is known prior to calculation, $\Sigma_0 = U/2$, and hence does not have to be determined self-consistently. Figure 3(a) shows the impurity spectral function $\rho(\omega) = -\mathrm{Im}G(\omega)/\pi$ for $U = 3$ and $\Gamma = 0.3$ calculated by DED with $n = 8$ sites, in comparison with the NRG spectrum. The DED and NRG spectra are in excellent overall agreement. The Anderson model is in the Kondo regime, where the spectral function is characterized by three resonances: The sharp Kondo resonance at the Fermi level and two Hubbard side peaks on either side of the Fermi level close to the excitation energies ϵ_d and $\epsilon_d + U$. In Fig. 3(b), we show DED spectra for different numbers of sites n in comparison with NRG for the same set of parameters as in Fig. 3(a). In order to better resolve the spectra at low energies, the energies are plotted on a logarithmic scale. Even for very small models ($n = 2$) there is good qualitative agreement with the NRG spectrum, but the width of the Kondo peak is overestimated by a factor of almost 3 [see also Fig. 3(h)], and the height of the Hubbard side peaks is slightly underestimated. Note, however, that the height of the Kondo peak $1/\pi\Gamma$ is always exact, independent of the number of sites n, since it is imposed by the particle constraint, as discussed in Sec. II B. As the number of sites n increases, the quantitative agreement with NRG improves considerably, becoming excellent for $n = 8$ sites. The quantitative improvement with increasing number of sites can also be seen in Fig. 3(h), where we show the half-width of the Kondo peak as a function of the model size n in comparison to the NRG value.

The number of randomly generated samples contributing to the ensemble average of the self-energy (13) generally determines the amount of noise in the spectra. For a fixed model size n, the noise can be reduced by increasing the number of samples N; it vanishes in the limit $N \to \infty$. On the other hand, the larger the number of sites n of the finite size, the fewer samples are needed to achieve the same level of noise, since the number of poles in the spectrum of individual samples increases. For example, in Fig. 3(b) for $n = 2,4,8$ sites about 5.8×10^4, 3.6×10^4, and 1.7×10^4 samples, respectively, were used to generate the spectra. In the limit $n \to \infty$ we would recover the continuous conduction band of the original Anderson model, and hence a single sample would already yield the exact and thus noiseless spectrum. In Table II in Appendix B we report the number of samples used in calculating the spectra shown in Figs. 3 and 4.

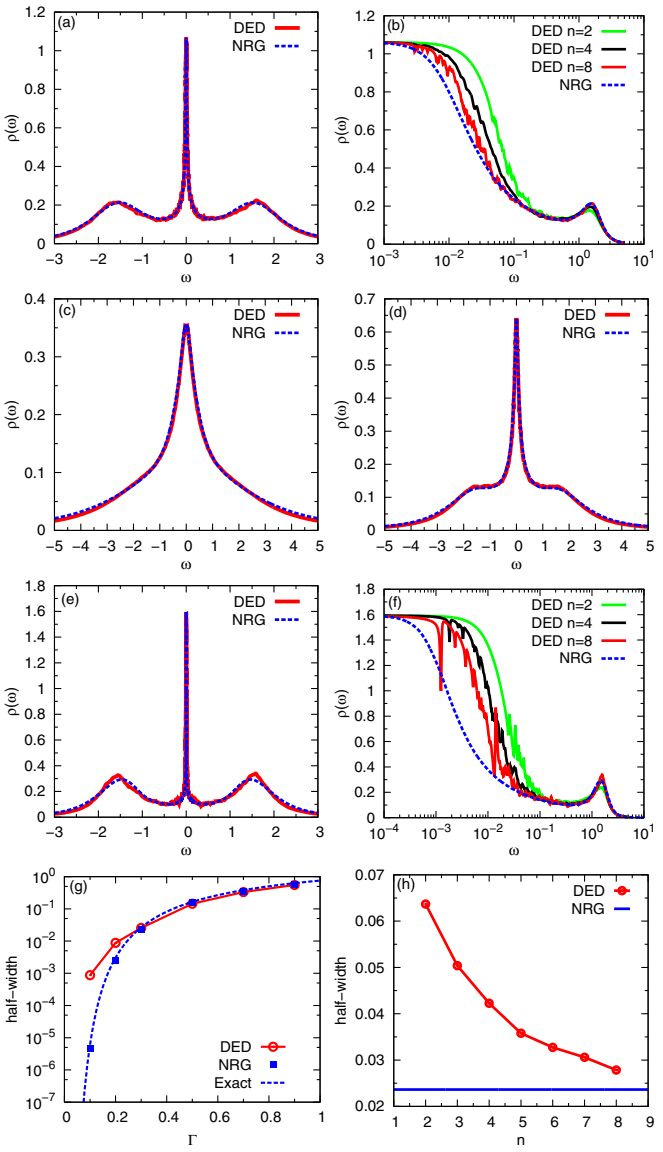

FIG. 3. Comparison between DED and NRG spectra for the symmetric Anderson model ($U = 3$, $\epsilon_d = -1.5$). (a) DED ($n = 8$) and NRG spectra for $\Gamma = 0.3$. (b) NRG and DED spectra with different number of sites n on a half-log scale for $\Gamma = 0.3$. (c) DED ($n = 6$) and NRG spectra for $\Gamma = 0.9$. (d) DED ($n = 6$) and NRG spectra for $\Gamma = 0.5$. (e) DED ($n = 8$) and NRG spectra for $\Gamma = 0.2$. (f) NRG and DED spectra for different number of sites n on a half-log scale for $\Gamma = 0.2$. (g) Half-width of Kondo peak estimated by fitting with Frota line shapes [45] versus Γ calculated by DED ($n = 8$ for $\Gamma \leqslant 0.3$ and $n = 6$ for $\Gamma \geqslant 0.5$) compared to NRG and the exact expression [46] on half-log scale. (h) Half-width of Kondo peak versus number of sites n compared to NRG for $\Gamma = 0.3$.

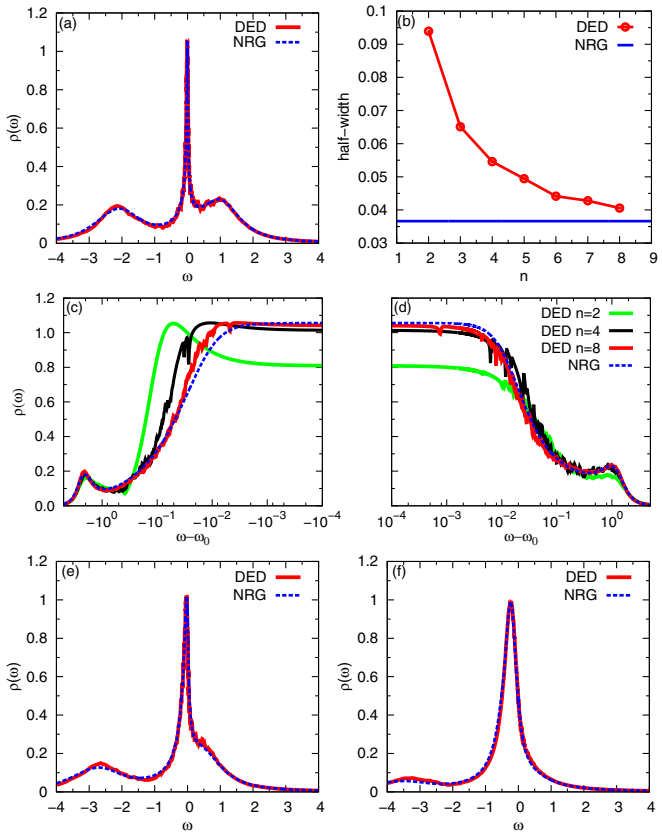

FIG. 4. Comparison between DED and NRG spectra for the asymmetric Anderson model ($U = 3, \epsilon_d < -1.5, \Gamma = 0.3$). (a) DED (for $n = 8$ sites) and NRG spectra for $\epsilon_d = -2$. (b) Half-width of Kondo peak versus number of sites n compared to NRG ($\epsilon_d = -2$). (c) NRG and DED spectra with different number of sites n for $\epsilon_d = -2$ on a half-log scale for negative energies. (d) NRG and DED spectra with different number of sites n for $\epsilon_d = -2$ on a half-log scale for positive energies. (e) DED (for $n = 8$ sites) and NRG spectra for $\epsilon_d = -2.5$. (e) DED (for $n = 8$ sites) and NRG spectra for $\epsilon_d = -3$.

Next we investigate how the quality of the DED spectra changes when the correlation strength controlled by U/Γ is altered. In Fig. 3(c) and 3(d) we show a comparison of spectra calculated by DED and NRG for higher values of the broadening Γ than before. For weak correlation strength [$\Gamma = 0.9$, Fig. 3(c)], the system is no longer in the Kondo regime: the spectra are characterized by a single peak, though different from the Lorentzian of the noninteracting system due to interaction effects. Here the agreement with NRG is excellent already for $n = 2$ (not shown). As the correlation strength increases, more sites are necessary to achieve good quantitative agreement. For $\Gamma = 0.5$ [Fig. 3(d)], we approach the Kondo regime, and the three-peak structure starts to emerge. Now excellent quantitative agreement with NRG can be achieved for $n = 6$ sites. We have discussed the case $\Gamma = 0.3$ [Figs. 3(a), 3(b), 3(h)] already in the Kondo regime, where excellent agreement with NRG is reached for $n = 8$ sites. Figures 3(e) and 3(f) show DED spectra in comparison with NRG for $\Gamma = 0.2$, on a normal energy scale [Fig. 3(e)], and on a logarithmic energy scale [Fig. 3(f)] for better resolution of the low-energy features. The overall qualitative agreement with the NRG spectrum is again quite good, as can be seen from Fig. 3(e). However, the quantitative agreement, especially of the low-energy features, i.e., the Kondo peak, is not very good anymore: the width of the Kondo peak is still strongly overestimated by almost a factor of 2 even for $n = 8$ sites. The high-energy features on the other hand are captured quite well, although the height of the Hubbard side peaks is slightly overestimated.

This behavior of decreasing quality of the DED at a fixed number of sites with increasing correlation strength U/Γ is summarized in Fig. 3(g) which shows the half-width of the Kondo peak as a function of Γ, comparing DED for $n = 8$ sites and NRG. For not too strong correlations, i.e., $\Gamma \geqslant 0.3$ ($U/\Gamma \leqslant 10$), DED for $n = 8$ sites yields an excellent approximation to the width of the Kondo peak, but begins to deviate from NRG as the correlations become stronger (decreasing Γ). For very strong correlations (i.e., $U/\Gamma \gg 10$), the width of the Kondo peak becomes strongly overestimated, by orders of magnitude [see also Fig. 3(e) and Fig. 3(f)]. This behavior can be understood by considering the Kondo screening cloud, whose spatial extension grows exponentially with increasing correlation strength [47]: $\xi_K \propto 1/T_K \propto e^{\Gamma/U}$. Thus the number of bath sites necessary to correctly describe the Kondo screening cloud grows exponentially with the correlation strength, leading generally to an overestimation of the Kondo temperature for too small bath sizes. Hence for very strong correlation strengths the DED method cannot provide a quantitatively satisfactory description of the spectra with a computationally feasible number of bath sites. Yet for correlation strengths up to and including $U/\Gamma \approx 10$ DED yields an excellent description of the spectra for small to moderate numbers of bath sites.

B. Asymmetric Anderson model

We now consider the AIM away from particle-hole symmetry, $\epsilon_d < -U/2$ and $\langle n_d \rangle > 1$. As explained before in Sec. II B, the parameter Σ_0 has to be determined self-consistently since we identified it with the real part of the self-energy at the Fermi level, $\Sigma_0 \equiv \mathrm{Re}\bar{\Sigma}(\epsilon_\mathrm{F})$, which is unknown prior to the DED calculation. We thus start with some reasonable initial guess, for example the Hartree shift $\Sigma_0 \equiv U\langle n_d \rangle/2$, calculated within Hartree-Fock, $\Sigma_0 \equiv U/2$, or simply $\Sigma_0 \equiv -\epsilon_d$. Using this Σ_0 in the DED procedure we calculate the self-energy $\bar{\Sigma}^{(1)}(\omega)$ and thus obtain a new guess for $\Sigma_0 \to \mathrm{Re}\bar{\Sigma}^{(1)}(\epsilon_\mathrm{F})$, and repeat until self-consistency is reached. This procedure usually converges within a few cycles (3–4) to an accuracy of under 1%. We find that the effect of the self-consistency on the overall spectrum is relatively small. The main effect is to improve the position of the Kondo peak and to recover the exact height of the Kondo peak. Hence if the fine details of the spectrum are less important, it suffices to compute $\bar{\Sigma}(\omega)$ for some reasonable guess, for example $\Sigma_0 = U/2$. More details on the self-consistent determination of Σ_0 can be found in Appendix C.

In Fig. 4(a) we show the impurity spectral density for $U = 3$, $\Gamma = 0.3$, and $\epsilon_d = -2$, calculated by DED for $n = 8$ sites in comparison with the NRG spectrum. The DED spectrum is in very good overall agreement with the NRG spectrum. For as much as we are in the Kondo regime the three-peak

structure is retained (see Sec. III A). As in the symmetric case, in order to better resolve the spectra at low energies, we use a logarithmic scale for the energy axis. Since here we are dealing with asymmetric spectra, we represent the spectral density on the logarithmic scale for negative and positive energies in Fig. 4(c) and Fig. 4(d), respectively. As in the ph-symmetric case, we observe quantitative improvement of the DED spectra with increasing n. Especially the position and width of the Kondo peak improve considerably: While for small n the peak is considerably offset from the Fermi level, the pinning of the Kondo peak to the Fermi level as seen in NRG is almost completely recovered for $n = 8$. As can be seen from Fig. 4(b), similarly to the symmetric case (see Sec. III A), the width of the Kondo peak is strongly overestimated for $n = 2$ by almost a factor of 3, but decreases rapidly with increasing n, until for $n = 8$ the width is only slightly overestimated by a few percent.

Next we investigate the quality of the DED spectra when moving away from the Kondo regime, by further decreasing ϵ_d such that $\epsilon_d + U$ approaches the Fermi level. In Figs. 4(e) and 4(f) we compare spectra calculated by DED (for $n = 8$ sites) and by NRG in the intermediate valence regime $\epsilon_d + U - \epsilon_F \approx \Gamma$. In this regime the charge of the impurity level fluctuates strongly between single and double occupation, leading to a significant deviation of $\langle n_d \rangle$ from unity. The spectral density is characterized by two resonances, one at $\approx \epsilon_d + U$ of width $\approx \Gamma$, and a much less pronounced resonance at ϵ_d. Upon further decreasing ϵ_d the resonance at ϵ_d becomes more strongly suppressed [compare Fig. 4(f) with Fig. 4(e)], as we get closer to the nonmagnetic regime ($\epsilon_d + U - \epsilon_F \ll -\Gamma$) where the impurity level is almost doubly occupied, and the resonance finally vanishes (not shown). As can be seen from Figs. 4(e) and 4(f), the DED spectra are in excellent agreement with the NRG ones even for strong asymmetry, capturing all the described features very well.

Finally, we also calculate the occupancy of the impurity level $\langle n_d \rangle$ for different values of ϵ_d and compare with NRG. We investigate two different ways of calculating $\langle n_d \rangle$ within DED. On the one hand we can calculate the occupancy from the ensemble average (ENS) over accepted finite Anderson model samples:

$$\langle n_d \rangle \approx \bar{n}_d = \frac{1}{N} \sum_{\nu} \langle 0^\nu | n_d | 0^\nu \rangle. \tag{22}$$

On the other hand we can make use of Friedel's sum rule (FSR), and calculate $\langle n_d \rangle$ from the self-energy at the Fermi level:

$$\langle n_d \rangle = 1 - \frac{2}{\pi} \tan^{-1} \left(\frac{\epsilon_d + \mathrm{Re}\bar{\Sigma}(\epsilon_\mathrm{F}) - \epsilon_\mathrm{F}}{\Gamma} \right), \tag{23}$$

where we have already taken into account spin degeneracy. Also note that $n_{\mathrm{imp},\sigma} = \langle n_{d,\sigma} \rangle$ in the flat-wide-band limit [2]. Table I shows the results for NRG and DED using $n = 8$ sites. The overall agreement between DED and NRG is very good. The values of $\langle n_d \rangle$ calculated by both approaches in DED agree with the NRG results within the statistical error [48] for all values of ϵ_d. However, the statistical error is generally smaller for the ENS approach. Only for very strong asymmetry ($\epsilon_d = -3$) does the error of the FSR approach become slightly smaller than the one of the ENS approach, and also the mean values are closer to the NRG results for ENS than for FSR.

TABLE I. The d-level occupancy $\langle n_d \rangle$ calculated by NRG compared to DED obtained (i) via the ensemble average (ENS) and (ii) via Friedel's sum rule (FSR) from $\mathrm{Re}\bar{\Sigma}(\epsilon_\mathrm{F})$ as well as the self-consistently determined $\Sigma_0 = \mathrm{Re}\bar{\Sigma}(\epsilon_\mathrm{F})$ for different values of ϵ_d and their statistical errors [48].

ϵ_d	NRG	DED (ENS)	DED (FSR)	Σ_0
-1.5	1.0000	0.9992 ± 0.0062	1.008 ± 0.068	1.496 ± 0.032
-1.65	1.0202	1.0234 ± 0.0063	1.039 ± 0.064	1.630 ± 0.030
-1.8	1.0420	1.0495 ± 0.0066	1.065 ± 0.057	1.769 ± 0.027
-2.0	1.0765	1.0862 ± 0.0089	1.132 ± 0.056	1.937 ± 0.027
-2.5	1.2322	1.2366 ± 0.0091	1.309 ± 0.035	2.341 ± 0.017
-3.0	1.5270	1.5364 ± 0.0128	1.533 ± 0.023	2.667 ± 0.012

From Table I we can see that the error in the occupancy $\langle n_d \rangle$ calculated via FSR as well as the error in Σ_0 decrease with increasing asymmetry. This can be understood by considering the acceptance ratio which becomes better the stronger the asymmetry (see Appendix B) so that more samples are accepted (for a fixed total number of samples) contributing to the ensemble average for the self-energy, and thus improving the statistics. For small asymmetries the argument to $\tan^{-1}$ in FSR (23) is close to zero [$\epsilon_d + \mathrm{Re}\bar{\Sigma}(\epsilon_\mathrm{F}) - \epsilon_\mathrm{F} \approx 0$], and therefore $\tan^{-1}$ has an approximately linear behavior so that $\delta n_d \approx \frac{2}{\pi\Gamma} \delta\Sigma_0$, explaining the factor of roughly two between the error in $\langle n_d \rangle$ and the error in Σ_0 since $2/\pi\Gamma \approx 2$ for $\Gamma = 0.3$. On the other hand, the error for $\langle n_d \rangle$ calculated via ENS *increases* slightly with increasing asymmetry despite more samples being accepted, since the occupancies of individual finite Anderson model samples fluctuate more strongly with increasing asymmetry.

IV. CONCLUSIONS

In conclusion, we find that DED generally yields an excellent description of the Anderson impurity model, inside as well as outside the Kondo regime. The spectra obtained by DED are in good qualitative agreement with NRG spectra already for a small number of bath sites. Depending on the correlation strength U/Γ excellent quantitative agreement can be achieved for a moderate number of 5–7 bath sites. Only for very strong correlation, $U/\Gamma \gg 10$, does the number of bath sites necessary to achieve a good quantitative description become too big to be computationally feasible due to the exponential growth of the Kondo screening cloud.

We further find that the particle number constraint plays an essential role in the DED method for the description of Kondo physics. Basically, the constraint ensures that individual finite Anderson model samples contributing to the self-energy average comply with Nozieres' Fermi liquid picture of the strong-coupling regime, thereby imposing Fermi liquid behavior on the sample-averaged self-energy. This leads to the recovery of the Kondo peak in the spectrum, which is absent in the DED procedure without the constraint.

The enforcement of Fermi liquid behavior by the constraint means that its role needs to be reconsidered when DED is applied to situations where Fermi liquid behavior is not obeyed, for example, at finite temperatures above T_K, in gapped systems, or in the case of multiorbital Anderson models where non-Fermi-liquid behavior may occur [49–51]. More precisely, it seems that the constraint needs to be relaxed in some way in order to describe the loss of Fermi liquid behavior in these cases. As can be seen from Fig. 2(a), without the constraint DED produces a spectrum similar to that of the Anderson model in the Coulomb blockade regime. In other words, DED with the constraint describes the strong-coupling fixed point of the Anderson model, while DED without the constraint seems to describe the weak-coupling fixed point. This may also explain why a DED+DMFT scheme without application of the constraint is capable of describing the gapped Mott-insulating phase of the Hubbard model [35]. Thus in order to describe the transition from the Fermi liquid to the Coulomb blockade or Mott regime a general principle for relaxing the constraint needs to be found.

An advantage of DED over NRG is that it can be parallelized very efficiently as the randomly generated finite Anderson model samples can be diagonalized independently from each other, and hence can be easily distributed over an arbitrarily large number of nodes. This recommends DED for the solution of multiorbital Anderson models which are not accessible for NRG for more than three impurity levels. Adopting the Lanczos diagonalization scheme in the DED procedure should allow one to treat multiorbital Anderson models with a sufficient number of bath sites per impurity level to achieve accurate results. Another advantage of DED is that the energy resolution is the same on all energy scales and thus can be exploited in resolving higher energy spectral features that would be difficult to resolve with NRG [35].

APPENDIX A: THE CONSTRAINT AND THE 1:1 CORRESPONDENCE WITH THE NONINTERACTING SYSTEM

As discussed in Sec. II B, the particle number constraint (14) ensures that every finite Anderson model sample contributing to the self-energy average (13) obeys Fermi liquid behavior, i.e., requires that a 1:1 correspondence can be established between the interacting model and the corresponding noninteracting effective model. In the following we discuss in more detail how this 1:1 correspondence is established via the constraint.

First, note that since each Anderson model sample ν is finite, the interacting and noninteracting particle numbers $n^\nu_{\rm imp}$ and $n^\nu_{{\rm imp},0}$, respectively, are discrete (integer) numbers, and thus also the corresponding phase shifts $\eta^\nu_\sigma(\epsilon_{\rm F})$ and $\eta^\nu_{0,\sigma}(\epsilon_{\rm F})$ are discrete numbers. Depending on the signs of the numerators in the arguments to $\tan^{-1}$ in Eqs. (16) and (20), the phase shifts can assume either the value 0 (negative) or π (positive), since for a finite system generally ${\rm Im}\Delta^\nu(\omega) \to 0$ as $\delta \to 0^+$ (unless ω is at a pole), and hence the argument to $\tan^{-1}$ diverges, i.e., goes to $\pm\infty$ depending on the sign of the numerator. A phase shift of $\pi/2$ is theoretically also possible (implying $n_{\rm imp} =$ 1), but in practice does not happen, as it means that either a bath level k is exactly at the Fermi level ($\epsilon^\nu_k = \epsilon_{\rm F}$), so that ${\rm Im}\Delta^\nu(\epsilon_{\rm F}) \to \infty$ as $\delta \to 0^+$, or the numerator is exactly zero, meaning that the sampled poles lie exactly symmetric with respect to the Fermi level. Hence during the DED procedure the phase shift of individual samples will fluctuate between the two values 0 and π. In the ph-symmetric situation ($\epsilon_d = -U/2$) the number of samples with phase shift 0 will be equal to the number of samples with phase shift π for a large enough number of samples. Hence on average we obtain the phase shift of $\pi/2$. Away from ph symmetry, the number of samples with one phase shift grows at the expense of samples with the other phase shift, leading to an average phase shift different from $\pi/2$.

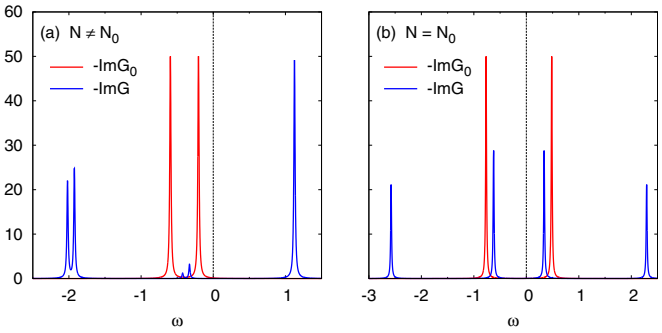

FIG. 5. Comparison of interacting (blue) and noninteracting (red) finite Anderson model spectra ($n = 2$ sites) for the case that (a) the particle constraint is not fulfilled, and (b) when it is fulfilled. Only in the latter case a 1:1 correspondence between the interacting and noninteracting system can be established.

The sign of the numerators $\epsilon_{\rm F} - \epsilon^\nu_d - {\rm Re}\Sigma^\nu_\sigma(\epsilon_{\rm F})$ in (16) and $\epsilon_{\rm F} - \epsilon^\nu_d - \Sigma_0$ in (20) are largely determined by the positions of the most important excitations with respect to the Fermi level. If the most important excitation is hole-like, then the numerator is negative and hence the phase shift is 0. If on the contrary the excitation is electron-like, the numerator is positive and hence leads to a phase shift of π. Therefore the constraint is only fulfilled (i.e., matching phase shifts of interacting and corresponding noninteracting systems) if the most important excitations in the interacting and noninteracting systems are of the same type, i.e., either both hole-like or both electron-like. This is illustrated in Fig. 5 which compares the spectra of an interacting and noninteracting finite Anderson model in the case that the constraint is not fulfilled (a) and when it is fulfilled (b). One can clearly see that the main excitations are not of the same type when the constraint is not fulfilled, while they are of the same type if the constraint is fulfilled. Clearly, in the latter case a 1:1 correspondence can be established between the excitations of the interacting and corresponding noninteracting systems.

APPENDIX B: DED STATISTICS

In Table II we summarize statistical information on the DED calculations reported in the text. One can see that the acceptance ratio $r_{\rm acc}$ increases with increasing Γ (i.e., decreasing correlation strength U/Γ), and increasing asymmetry. In both cases interaction effects become weaker, so that the

TABLE II. Summary of statistical information of the DED calculations reported in the text. Total number of samples $N_{\rm tot}$, number of accepted samples $N_{\rm acc}$, and the acceptance ratio $r_{\rm acc}$ for different values of ϵ_d, Γ, and number of sites n. For all calculations $U = 3$ was used.

ϵ_d	Γ	n	$N_{\rm tot}$	$N_{\rm acc}$	$r_{\rm acc}$
−1.5	0.2	8	23 875	7449	31%
−1.5	0.3	2	2 00 000	57 561	29%
−1.5	0.3	4	1 00 000	35 918	36%
−1.5	0.3	8	38 594	16 504	43%
−1.5	0.5	6	1 00 000	55 066	55%
−1.5	0.9	6	1 00 000	70 297	70%
−1.65	0.3	8	8500	3743	44%
−1.8	0.3	8	8495	3847	45%
−2.0	0.3	8	8495	4037	47%
−2.5	0.3	8	7958	4809	60%
−3.0	0.3	8	8000	6452	81%

noninteracting limit is approached, where the DED becomes exact already for the one-site model [the noninteracting DOS can be reproduced by simply sampling the noninteracting DOS $\rho_0(\omega)$ of course] where the constraint is always fulfilled.

APPENDIX C: SELF-CONSISTENT DETERMINATION OF Σ_0

As explained in Sec. II B the effective one-body potential Σ_0 entering the noninteracting GF (3) should be identified with the real part of the self-energy at the Fermi level, $\Sigma_0 \equiv \mathrm{Re}\Sigma(\epsilon_{\rm F})$. However, with the exception of the ph-symmetric situation where $\mathrm{Re}\Sigma(\epsilon_{\rm F}) = U/2$, the self-energy at the Fermi level is unknown prior to calculation. Hence we propose to determine

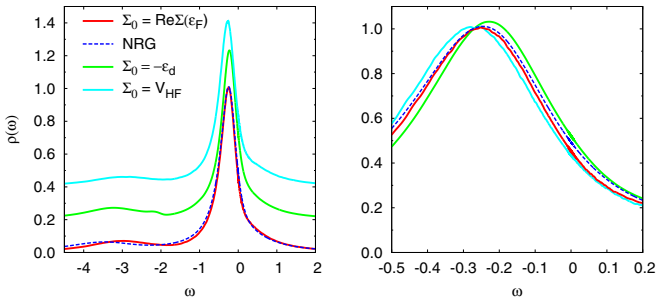

FIG. 6. Spectral function close to the Fermi level for different values of Σ_0 calculated by DED ($n = 4$ sites) compared to NRG for $U = 3$, $\epsilon_d = -3$, and $\Gamma = 0.3$ on a large energy scale (left) and at low energies (right). Note that on the left panel the curves for $\Sigma_0 = -\epsilon_d$ (green) and for $\Sigma_0 = V_{\rm HF}$ (cyan) have been offset by 0.2 and 0.4, respectively, in order to increase the visibility.

Σ_0 self-consistently, by starting with some initial guess, e.g., $\Sigma_0 \to U/2$. Using this initial guess the DED procedure yields $\mathrm{Re}\bar{\Sigma}(\epsilon_{\rm F})$, generally different from Σ_0, which is taken as the new guess, $\Sigma_0 \to \mathrm{Re}\bar{\Sigma}(\epsilon_{\rm F})$. This procedure is repeated until self-consistency is reached, i.e., Σ_0 does not change anymore within a specified accuracy. We find that the self-consistency converges quite rapidly to an accuracy of under 1% within 3–4 cycles. In Fig. 6 we show the effect of the self-consistency for Σ_0 on the spectra close to the Fermi level. The agreement between NRG and DED using the converged value $\Sigma_0 = \mathrm{Re}\bar{\Sigma}(\epsilon_{\rm F}) \approx 2.65$ (red line) is quite good. But the effect of self-consistency is actually relatively weak: DED with the initial guess $\Sigma_0 = -\epsilon_d$ or using the Hartree shift for Σ_0 yield spectra that are also quite close to the NRG spectrum, with the peak position just slightly shifted, even when using the Hartree-Fock potential $\Sigma_0 \equiv V_{\rm HF} \approx 2.49$ (cyan line).

[1] P. W. Anderson, Phys. Rev. **124**, 41 (1961).
[2] A. C. Hewson, *The Kondo Problem to Heavy Fermions* (Cambridge University Press, Cambridge, 1997).
[3] W. Metzner and D. Vollhardt, Phys. Rev. Lett. **62**, 324 (1989).
[4] A. Georges and G. Kotliar, Phys. Rev. B **45**, 6479 (1992).
[5] A. Georges, G. Kotliar, W. Krauth, and M. J. Rozenberg, Rev. Mod. Phys. **68**, 13 (1996).
[6] G. Kotliar, S. Y. Savrasov, K. Haule, V. S. Oudovenko, O. Parcollet, and C. A. Marianetti, Rev. Mod. Phys. **78**, 865 (2006).
[7] R. Bulla, T. A. Costi, and T. Pruschke, Rev. Mod. Phys. **80**, 395 (2008).
[8] E. Gull, A. J. Millis, A. I. Lichtenstein, A. N. Rubtsov, M. Troyer, and P. Werner, Rev. Mod. Phys. **83**, 349 (2011).
[9] N. Grewe and H. Keiter, Phys. Rev. B **24**, 4420 (1981).
[10] P. Coleman, Phys. Rev. B **29**, 3035 (1984).
[11] T. Pruschke and N. Grewe, Z. Phys. B **74**, 439 (1989).
[12] K. Haule, S. Kirchner, J. Kroha, and P. Wölfle, Phys. Rev. B **64**, 155111 (2001).
[13] T. A. Costi, J. Kroha, and P. Wölfle, Phys. Rev. B **53**, 1850 (1996).
[14] N. Grewe, S. Schmitt, T. Jabben, and F. B. Anders, J. Phys.: Condens. Matter **20**, 365217 (2008).
[15] K. Yosida and K. Yamada, Prog. Theor. Phys. **46**, 244 (1970).
[16] N. Read and D. M. Newns, J. Phys. C **16**, L1055 (1983).
[17] D. E. Logan, M. P. Eastwood, and M. A. Tusch, J. Phys.: Condens. Matter **10**, 2673 (1998).
[18] A. C. Hewson, J. Phys.: Condens. Matter **13**, 10011 (2001).
[19] Q. Feng and P. M. Oppeneer, J. Phys.: Condens. Matter **23**, 425601 (2011).
[20] M. Caffarel and W. Krauth, Phys. Rev. Lett. **72**, 1545 (1994).
[21] A. Liebsch and H. Ishida, J. Phys.: Condens. Matter **24**, 053201 (2012).
[22] O. Újsághy, J. Kroha, L. Szunyogh, and A. Zawadowski, Phys. Rev. Lett. **85**, 2557 (2000).
[23] J. Li, W.-D. Schneider, R. Berndt, and B. Delley, Phys. Rev. Lett. **80**, 2893 (1998).
[24] V. Madhavan, W. Chen, T. Jamneala, M. F. Crommie, and N. S. Wingreen, Science **280**, 567 (1998).
[25] H. C. Manoharan, C. P. Lutz, and D. M. Eigler, Nature (London) **403**, 512 (2000).
[26] N. Knorr, M. A. Schneider, L. Diekhöner, P. Wahl, and K. Kern, Phys. Rev. Lett. **88**, 096804 (2002).
[27] P. Wahl, L. Diekhöner, M. A. Schneider, L. Vitali, G. Wittich, and K. Kern, Phys. Rev. Lett. **93**, 176603 (2004).

[28] N. Néel, J. Kröger, L. Limot, K. Palotas, W. A. Hofer, and R. Berndt, Phys. Rev. Lett. **98**, 016801 (2007).
[29] L. Vitali, R. Ohmann, S. Stepanow, P. Gambardella, K. Tao, R. Huang, V. S. Stepanyuk, P. Bruno, and K. Kern, Phys. Rev. Lett. **101**, 216802 (2008).
[30] B. Surer, M. Troyer, P. Werner, T. O. Wehling, A. M. Läuchli, A. Wilhelm, and A. I. Lichtenstein, Phys. Rev. B **85**, 085114 (2012).
[31] D. Jacob, J. Phys.: Condens. Matter **27**, 245606 (2015).
[32] P. P. Baruselli, R. Requist, A. Smogunov, M. Fabrizio, and E. Tosatti, Phys. Rev. B **92**, 045119 (2015).
[33] S. Frank and D. Jacob, Phys. Rev. B **92**, 235127 (2015).
[34] M. Granath and H. U. R. Strand, Phys. Rev. B **86**, 115111 (2012).
[35] M. Granath and J. Schött, Phys. Rev. B **90**, 235129 (2014).
[36] Y. Lu, M. Höppner, O. Gunnarsson, and M. W. Haverkort, Phys. Rev. B **90**, 085102 (2014).
[37] M. Schüler, C. Renk, and T. O. Wehling, Phys. Rev. B **91**, 235142 (2015).
[38] In the case of a degenerate ground state the GF would be obtained from the corresponding ensemble average over the ground state manifold. Note, however, that the particle constraint discussed in Sec. II B ensures that the ground state is actually a singlet state.
[39] J. S. Langer and V. Ambegaokar, Phys. Rev. **121**, 1090 (1961).
[40] D. C. Langreth, Phys. Rev. **150**, 516 (1966).
[41] P. Nozières, J. Low Temp. Phys. **17**, 31 (1974).
[42] R. Žitko, available at http://nrgljubljana.ijs.si.
[43] R. Žitko and T. Pruschke, Phys. Rev. B **79**, 085106 (2009).
[44] R. Bulla, T. A. Costi, and D. Vollhardt, Phys. Rev. B **64**, 045103 (2001).
[45] H. O. Frota, Phys. Rev. B **45**, 1096 (1992).
[46] T. A. Costi, A. C. Hewson, and V. Zlatic, J. Phys.: Condens. Matter **6**, 2519 (1994).
[47] I. Affleck, The Kondo screening cloud, in *Strongly Correlated Fermions and Bosons in Low-Dimensional Disordered Systems*, edited by I. V. Lerner, B. L. Althsuler, V. I. Fal'ko, and T. Giamarchi (Springer Netherlands, Dordrecht, 2002), pp. 1–12.
[48] The statistical errors of the ensemble-averaged occupancy and of Σ_0 were estimated from the standard deviation from the mean over all accepted samples. In the case of the occupancy calculated from Σ_0 by FSR, the statistical error was calculated by error propagation from the standard deviation of Σ_0, i.e., $\delta n_d = |\partial n_d/\partial \Sigma_0|_{\Sigma_0} \delta \Sigma_0$.
[49] P. Noziéres and A. Blandin, J. Phys. **41**, 193 (1980).
[50] P. Schlottmann and P. D. Sacramento, Adv. Phys. **42**, 641 (1993).
[51] L. De Leo and M. Fabrizio, Phys. Rev. B **69**, 245114 (2004).